CLASSIFICATION OF SURFACE WATER AREA FROM MULTISPECTRAL AND MULTISAR DATA USING AUTOMATIC AND ROBUST SYSTEM

Husniyah Binti Mahmud (1), Masahiko Nagai (1)

[1] Yamaguchi University, 2 Chome-16-1 Tokiwadai, Ube, Yamaguchi 755-8611, Japan
Email: i504wd@yamaguchi-u.ac.jp; nagaim@yamaguchi-u.ac.jp

KEY WORDS: MultiSAR, Multispectral, Automatic Classification, Surface water extent, Google Earth Engine

ABSTRACT: Malaysia experienced flood almost every year, however, rain gauge and weather radar used to observe flood are not adequate. Satellite like Synthetic Aperture Radar (SAR) and multispectral imaging could potentially use to support classifying water areas. However, frequent monitoring combining this individual image could result in inconsistent water area output by time. Since processing big data is a time-consuming and labor-intensive task, a fully automatic and robust approach image classification is required. The objective of this study is to develop an automatic and robust method to spatially and temporally classify surface water from a set of a continuous multi-satellite dataset based on the 2017 North region flood case in Malaysia and secondly, to reduce their inconsistency when integrated. In this study, we use an automated flood extraction system by using weight averages of Neighborhood Valley-Emphasis Otsu's threshold values on the total backscatter of HH and HV of ALOS-2 images and total backscatter of VV and VH of Sentinel-1 images. An automatic Otsu thresholding from four different water indexes used to extract surface water from multispectral images. These water indexes are NDWI, MNDWI, AWEInsh, and AWEIsh and the best selected to delineate surface water extent from multispectral images. This automatic classification implemented using the Google Earth Engine platform. The result shows that MNDWI is the best water index for automatic delineation of surface water extent for Landsat 7, Landsat 8, and MODIS while NDWI is use to automatically delineate surface water extent from Sentinel 2 images. The result also shows that the extracted surface water from multispectral images using the OTSU threshold from a stable water index can successfully reduce the inconsistency with a set of multiSAR images when integrated. The model can be very useful in quickly understanding the changes in water bodies by the time during flood events from multi-satellite, but further validation is required for accurate mapping.

1. INTRODUCTION

In Malaysia, floods occur almost annually and bring the greatest damage. The topography and drainage of Malaysia including its human settlement and land-use patterns causing Malaysia to be very prone to flood risk. In general, flood in Malaysia classified into four types, which are "flash flood", "monsoonal flood", "river flood" and "tidal flood". Flash floods are most commonly occur in the urban area. Flood frequency and magnitude have been increasing due to the rapid development around river basins, which has cause river capacity to reduce in this current year. Flash flood has been severe and a serious problem in the urban area. During the monsoon season, Malaysia receives an average of more than 3000 mm of rainfall. Riverine and lowland coastal areas are highly exposed to flood risk. Tidal floods also one of the factor of a major flood in a coastal area and the flood become severe when the high tide occurs at the same time with heavy rains or strong wind. Major flood recorded in Malaysia area in the years 1926, 1963, 1965, 1967, 1969, 1971, 1973, 1979, 1983, 1988, 1993, 1998, 2005, December 2006, January 2007, 2010, 2014. 2017 and 2019.

Surface water can be defined as any water body found on the surface of the earth, this includes a freshwater lake, river and streams, and saltwater in the ocean. The changes in surface water mapping are a significantly important parameter for the application of water resources and natural hazard management during flood events. Patterns of flooding and flood risk and its impact can be described based on surface water extend mapping. Flood extend map can be acquired from both optical satellite

images and Synthetic Aperture Radar (SAR) images.

There is four common water classification method from optical remote sensing images (Ji et al., 2009). Which are thematic classification (Lira, 2006), linear unmixing (Sethre, Rundquist, & Todhunter, 2005), single-band thresholding (Jain, Singh, Jain, & Lohani, 2005), and two-band spectral water indices (Jain et al., 2006, McFeeters, 1996, Rogers and Kearney, 2004, Xu, 2006). The most common method used for water extraction is thresholding from single and two-band indices because this method required less time to complete (Ryu, Won, & Min, 2002). Manual classifications are relatively slow and subjective to bias due to misinterpretation of the satellite images.

There are several water indexes used to delineate open water features, which are Normalized Difference Water Index (NDWI), Modified Normalized Difference Water Index (MNDWI), and Automated Water Extraction Index (AWEI). NDWI uses green and near infrared (NIR) to delineate water features (McFeeters, 1996). (Xu, 2006) proposed MNDWI where a normalized difference of green and shortwave infrared (SWIR) band is used to overcome the limitations of NDWI which are NDWI cannot efficiently discriminate built-up surfaces signal and 0 value of threshold from NDWI cannot accurately distinguish water and built-up pixels. By using SWIR better water feature detection can be obtained because SWIR is more sensitive to the NIR. However, these two water indexes not made to separate water shadow surfaces. (Feyisa *et al*., 2014) proposed another two versions of water indexes, which are AWEInsh an automated water extraction index with no shadow, and AWEIsh an automated water extraction index with shadow.

Google Earth Engine (GEE) is a Google cloud geospatial processing service. GEE is more convenient than traditional geospatial processing service since it is open for public, simple algorithm development, and able to process the batch of satellite image data. By using this platform, big data geospatial images can be processed and analyze with less time consuming and less laborious task.

The objectives of this study are first, to develop a stable an automatic, and robust method to spatially and temporally classify surface water from a set of continuous data of multi-satellite based on the 2017 North region flood case in Malaysia and secondly, to reduce their inconsistency when combined.

2. MATERIALS AND METHODS

2.1 Study area

Perlis is located at latitude 6° 26' 36.9204" N and longitude 100° 12' 59.7564" E as shown in Figure 1. The total area of Perlis is 819 km² and a catchment area of 724.4 km². Perlis is comprised of three districts, which are Arau, Kangar, and Padang Besar. The topography of Perlis mostly flat with less than 61 meters above sea level. Perlis experience rainfall from April to May and August to October with average rainfall per year ranges between 1704 mm and 2005 mm. In this study, only Arau and Kangar chose a study area because of only these two areas reported in the Department of Irrigation and Drainage Flood Annual Report 2017/2018 facing flood twice in the year 2017/2018.

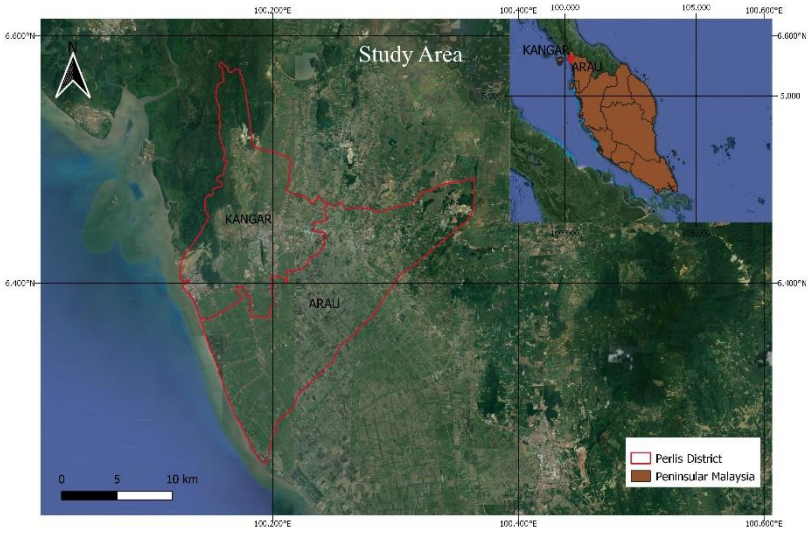

Figure 1 Location of the study area

2.2 Data used

The main data sources in this study decided based on a flood case in September 2017. Continuous heavy rainfall starts on 15 September 2017 and continues until early October 2017. This is due to the current atmosphere in a wet condition all week and due to the influence of Typhoon Doksuri, which is located in the north of Vietnam on 15th September. In general, during this time, Malaysia is at the end of the southwest monsoon and it is in a weak state. Typhoon Doksuri causing the concentrated wind direction and high humidity causing continuous heavy rainfall for two weeks. Besides, a big high tide phenomenon that happens at the same time with heavy rainfall causing the major flood to occur. Any available Multispectral and MultiSAR images from 1st September to 31st October are selected to create a frequent mapping of surface water extent.

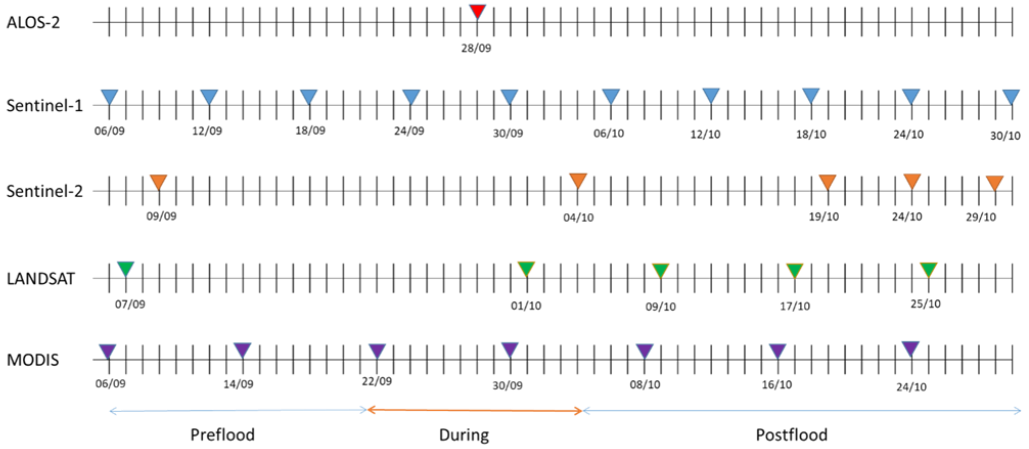

Figure 2 Temporal coverage of ALOS-2, Sentinel-1, Sentinel-2, Landsat 7, Landsat 8, and MODIS data acquired over the study area during the flood event.

MultiSAR used in this study are images from ALOS-2 and Sentinel-1 satellites. The ALOS-2 image use in this study is a high sensitive 6m resolution image with 14 days revisit time. We used both HH and HV of the 28th September 2017 image and it is in the ascending mode. Sentinel-1 is a C-band SAR data with a revisit time of 6 days and high spatial resolution with a resolution of 10 m. We use VV and VH polarization from each image and both ascending descending images are included to achieve high temporal coverage.

Multispectral images are from Sentinel-2, Landsat-7, Landsat-8, and MODIS MOD09A1. Sentinel-2 revisit period is five days. Sentinel-2B launched on March 7, 2017. The Sentinel-2 image has a different spatial resolution on each band. Due to its different spatial resolution size for the SWIR

band, we decide only use NDWI on the Sentinel-2 image. We use only green band B3 (560 nm) and its near infrared is B8 (842 nm) with both 10m spatial resolution.

For Landsat 7 carries the Enhanced Thematic Mapper Plus (ETM+) sensor and has acquired and delivered data with data gaps caused by the Scan Line Corrector (SLC) failure. It has 30 m spatial resolution and the image we utilized in this study are Band 1 Visible (0.45 - 0.52 µm), Band 2 Visible (0.52 - 0.60 µm), Band 4 Near-Infrared (0.77 - 0.90 µm), Band 5 Short-wave Infrared (1.55 - 1.75 µm) and Band 7 Mid-Infrared (2.08 - 2.35 µm).

Meanwhile, Landsat 8 carries the Operational Land Imager (OLI) and the Thermal Infrared Sensor (TIRS) instruments. Band 2 Visible (0.450 - 0.51 µm), Band 3 Visible (0.53 - 0.59 µm), Band 5 Near-Infrared (0.85 - 0.88 µm), Band 6 SWIR 1(1.57 - 1.65 µm) and Band 7 SWIR 2 (2.11 - 2.29 µm). All of these images are 30 m resolution.

The MODIS Terra MOD09A1 is an 8-day product (http://LPDAAC.usgs.gov) starting from the 6 September 2017 used in this study. The layers used from the MOD09A1 product are the surface reflectance band 2 (841-876 nm), surface reflectance band 3 (459-479 nm), surface reflectance band 4 (545-565 nm), surface reflectance band 5 (1230-1250 nm), and surface reflectance band 6 (1628-1652 nm). All of these multispectral images data are available on GEE, which enables a quick and multi-scale analysis.

2.3 Flood classification from MultiSAR

The proposed methodology for multi-temporal cloud detection based on our previous work (Husniyah & Masahiko, 2019). The extraction of surface water from SAR images are categorized into pre-processing, selection of water references, automatic thresholding using python, selection of bimodal histogram from the water references then we extract the surface water based on the average value of threshold of water references with histogram with bimodal shape then finally, we crop the region of interest and calculate the area of surface water.

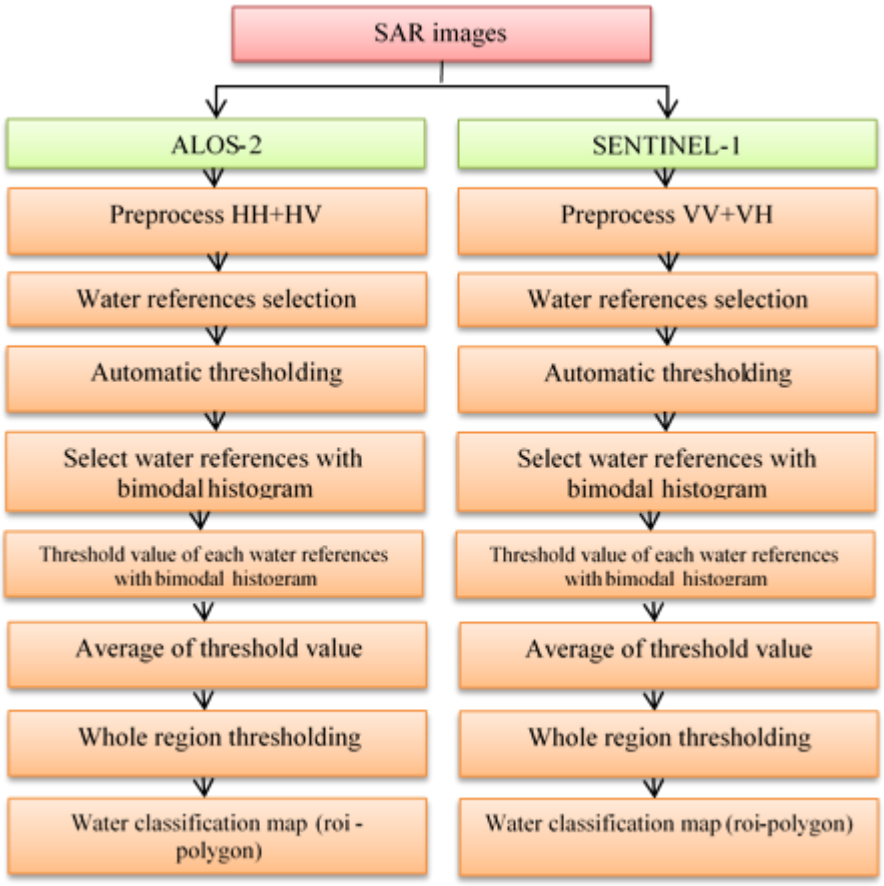

Figure 3 Flowchart for Sentinel-1 and ALOS-2 image processing.

2.4 Flood classification from Multispectral

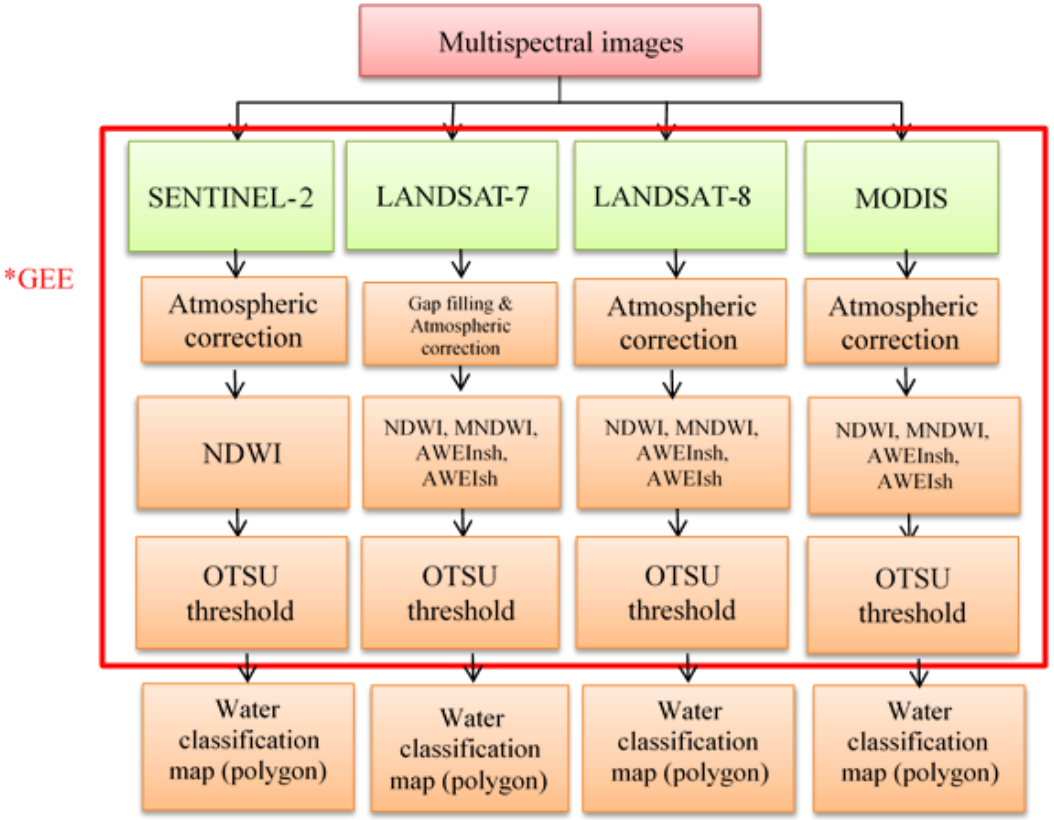

Figure 4 Flowchart for Sentinel-2, Landsat-7, Landsat-8, and MODIS image processing.

Figure 4 shows a framework using the Google Earth Engine platform automatically extract surface water with the Sentinel-2, Landsat 7, Landsat 8, and MODIS data.

We select four water indexes to extract surface water from remotely sensed data, which are Normalized Difference Water Index (NDWI) (Gao, 1996), the Modified Normalized Difference Water Index (MNDWI), and the Automated Water Extraction Index (AWEIsh) shadow and Automated Water Extraction Index (AWEInsh) no shadow. We used the Otsu threshold adjustment algorithm, which is widely used in water extraction to test the extraction effect of different water-indexing methods on the surface water extent. The best delineation chosen to represent the water index for future study.

2.4.1 Image processing using Otsu threshold

Gennadii et al. (2016) proposed the unsupervised classification step based on the local adaptive threshold detection method. The segmentation of the water from the spectral index was build based on the extension of the Otsu method by a Canny edge filter where the number of input pixels only to those located near water-land edges. Using the morphological dilation, water and land pixels located near water computed and applied to the detected edges. In the case of thin, single-pixel wide water bodies' skewed distribution might be obtained. A buffer size (dilation) equal to half of the pixel is used to overcome the problem. A bimodal distribution is expected so that a clear distinction of land and water can be acquired.

Using the following parameters: $\sigma = 0.7$, the = 0.99 for the Canny edge filter, and a structuring element with the size 15 m × 15 m to dilate the edges and create a surrounding buffer region in a case of two classes in the grid tile, we were able to get an almost perfect detection of water pixels. The σ and th parameters are used to define the standard deviation of the Gaussian smoothing kernel and the threshold used to define the sensitivity of the filter, respectively.

3. RESULTS AND DISCUSSIONS

3.1 Flood classification from MultiSAR

Figure 5 shows the extracted water mask from Sentinel-1 and ALOS-2 overlay on Google satellite image along the river line of the Perlis River.

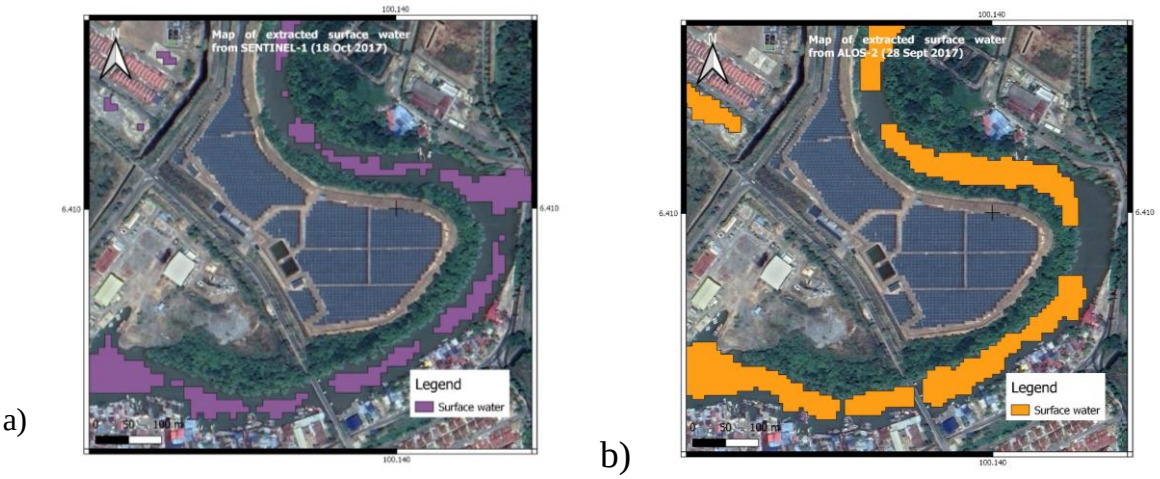

a) b)

Figure 5 Visual comparison of sample result from a) overlay of water mask extracted from Sentinel-1 and b) overlay of water mask extracted from ALOS-2.

The extraction result shows that both can distinguish water area from the land area. ALOS-2 shows better coverage and continuous pixel detection for the river line than Sentinel-1. Sentinel-1 shows patchy and small water segment as compared to ALOS-2. Both images can separate the built up which is a road located across the river. However, ALOS-2 has difficulty to detect water when the river line is bending.

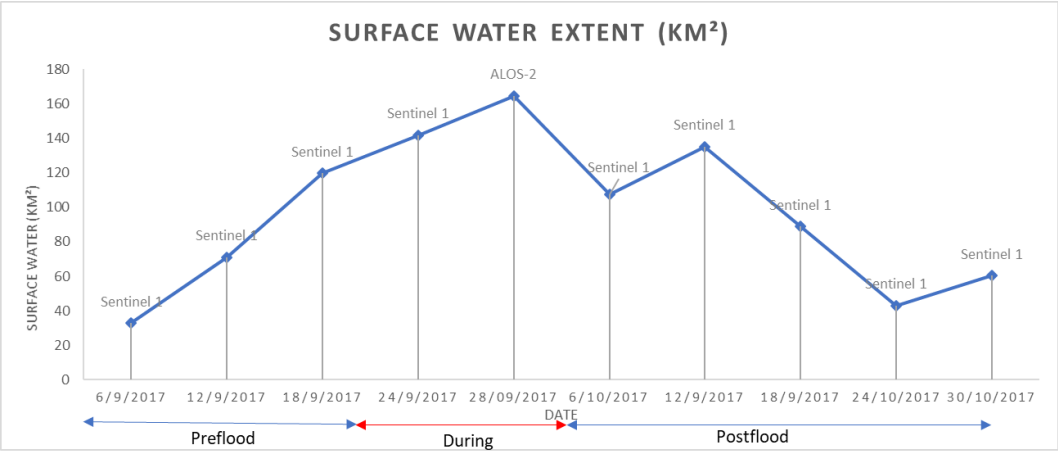

Figure 6 Changes of surface water extent in the study area from Sentinel-1 and ALOS-2 data between 06/09/2017 to 30/10/2017.

The changes of the surface water extent during the flood event shown in Figure 6. For this purpose, 11 radar satellites covered the study area has been used (10 Sentinel-1 and 1 ALOS-2). The classification result shows that during preflood, which was from 06/09/2017 to 18/09/2017 the surface water record from 32.92 km² gradually, increase from 71.10 km² to 119.73 km². By the time after flood starts on 21st September, the Sentinel-1 image on 24/09/2017 shows 141.86 km² of total surface water area and increase to 164.54 km² classified based on ALOS-2 image. After the flood ended in the early October estimate on 4th October, the surface water extent gradually decreases from 107.47 km² to 60.29 km² at the end of October.

3.2 Flood classification from MultiSAR

Satellite	True-color image	NDWI	MNDWI	AWEInsh	AWEIsh
LANDSAT 7 (07 SEPT)					
LANDSAT 8 (01 OCT)					
SENTINEL 2 (24 SEPT)	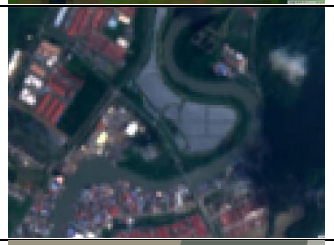				
MODIS MOD09A1 (30 SEPT)	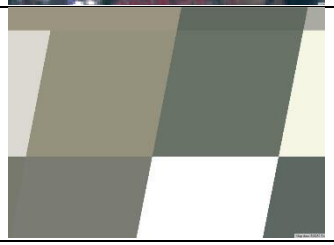				

Figure 7 Visual comparison of sample image of optical data showing classified Perlis River area from each water index.

3.3 Flood classification from Multispectral

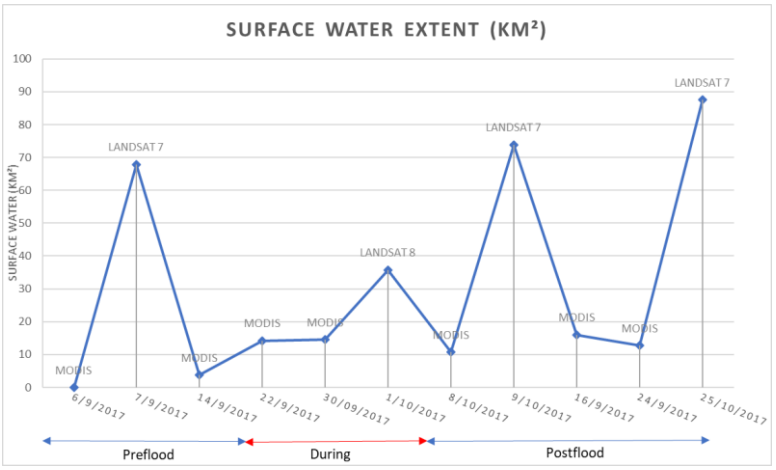

Figure 8 Changes of surface water extent in the study area from Landsat 7, Landsat 8, and MODIS data between 06/09/2017 to 30/10/2017 based on NDWI.

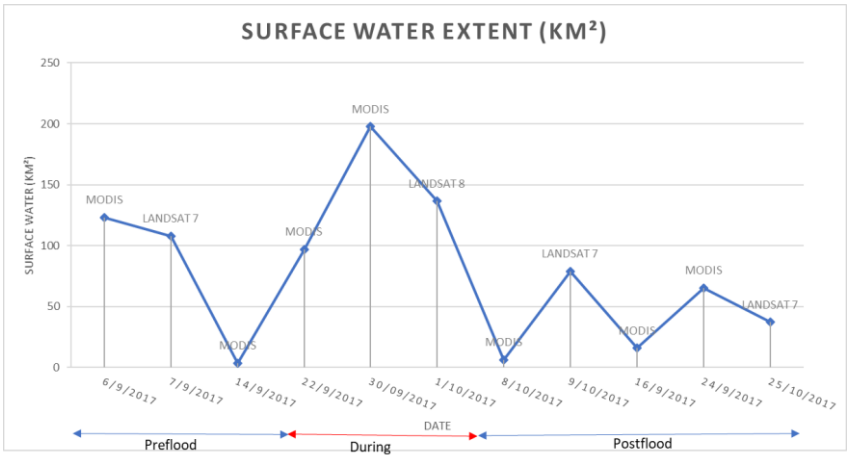

Figure 9 Changes of surface water extent in the study area from Landsat 7, Landsat 8, and MODIS data between 06/09/2017 to 30/10/2017 based on MNDWI.

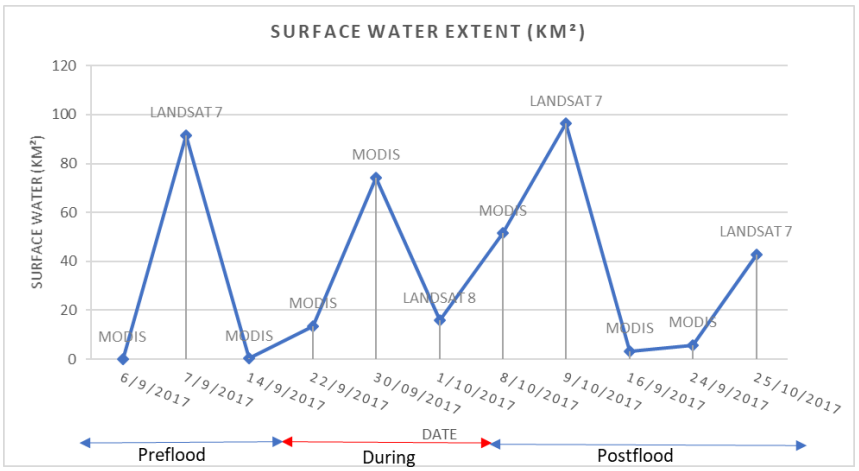

Figure 10 Changes of surface water extent in the study area from Landsat 7, Landsat 8, and MODIS data between 06/09/2017 to 30/10/2017 based on AWEInsh.

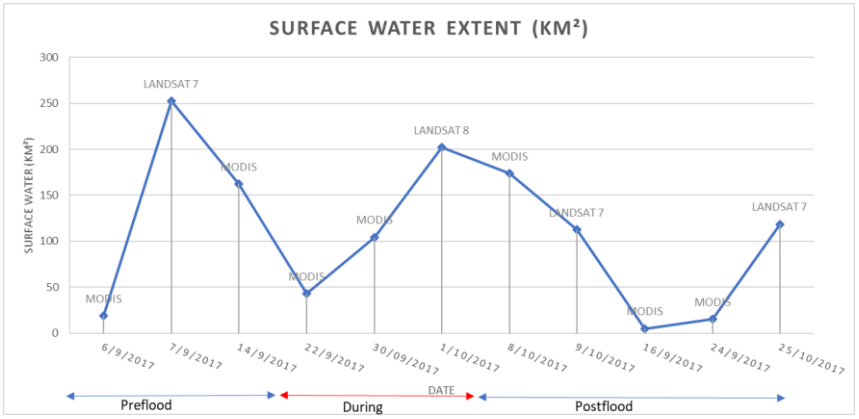

Figure 11 Changes of surface water extent in the study area from Landsat 7, Landsat 8, and MODIS data between 06/09/2017 to 30/10/2017 based on AWEIsh.

Figure 8 to 11 shows the changes of classified surface water extent from Landsat 7, Landsat 8, and MODIS by the time during the flood event using the threshold of NDWI, MNDWI, AWEInsh, and AWEIsh. Based on the assessment, other water indices shows a poor performance compare to MNDWI. MNDWI selected to represent the water index for Landsat 7, Landsat 8, and MODIS.

3.4 Integration of MultiSAR and Multispectral

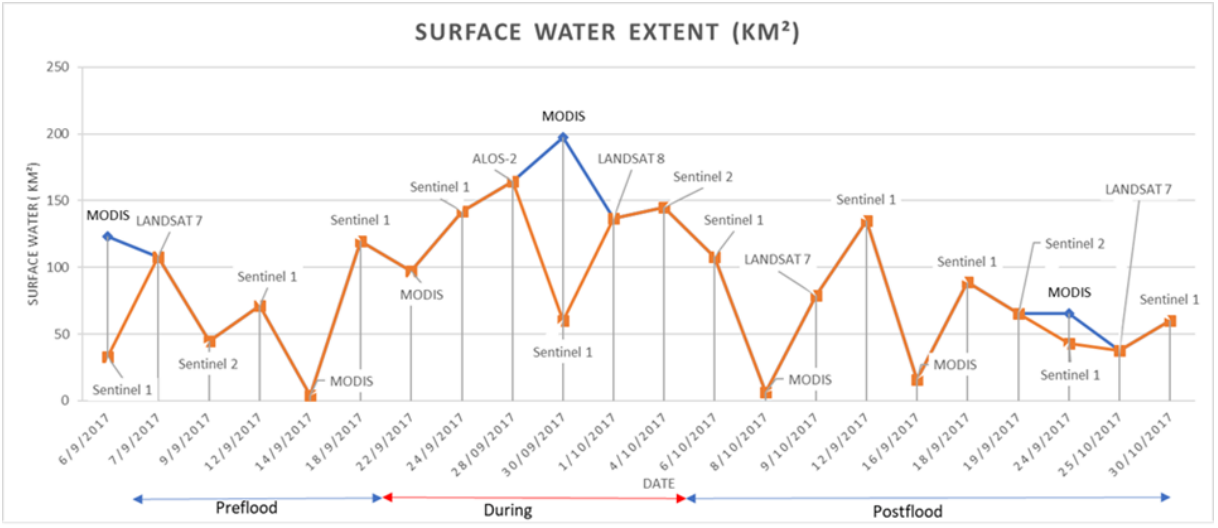

Figure 12 Changes of surface water extent in the study area from Sentinel-1, ALOS-2, Sentinel-2, Landsat 7, Landsat 8, and MODIS data between 06/09/2017 to 30/10/2017.

Figure 12 shows the changes of surface water extent using combination of various multi-satellite. The dataset shows a distinct preflood, during, and post flood of surface water area. Overall, there is a distinctive trend in the total areas of water surfaces during flood, where it reached it maximum during flood event. The model can be very useful in quickly understanding the changes in water bodies by the time during flood events from multi-satellite, but further validation is required for accurate mapping.

4. CONCLUSION

This paper has discussed the technique for automatic extraction of the flooded area, calculating the surface water extent and integrate SAR and optical images. Finally, based on the analysis, MNDWI and optical images on google earth platform useful for a frequent and rapid water surface monitoring. For the future work, we would like to do a fusion on satellite image captured at the same date, which

in this study is MODIS and Sentinel-1 image. We also will validate the surface water extent with ground truth data and use the extracted surface water result for further flood application study.

References from Journals:

Donchyts, G.; Schellekens, J.; Winsemius, H.; Eisemann, E.; Van de Giesen, N. A 30 m Resolution Surface Water Mask Including Estimation of Positional and Thematic Differences Using Landsat 8, SRTM and OpenStreetMap: A Case Study in the Murray-Darling Basin, Australia. *Remote Sens.* 2016, *8*, 386.

Feyisa, G. L., Meilby, H., Fensholt, R. & Proud, S. R. Automated water extraction index: A new technique for surface water mapping using Landsat imagery. Remote Sensing of Environment 140, 23–35 (2014).

Fisher, A.; Danaher, T. A water index for SPOT5 HRG Satellite imagery, New South Wales, Australia, determined by linear discriminant analysis. *Remote Sens* 2013, *5*, 5907–5925.

Husniyah Binti Mahmud & Masahiko Nagai. Automated Extraction Of Flood For Large Scale Area Using Weight Average Otsu's Method From Alos-2 Dual Polarization And Modis. The 40th Asian Conference on Remote Sensing (ACRS 2019), October 14-18, (2019).

Jain, S.K., A.K. Saraf, A. Goswami, and T. Ahmad, 2006. Flood inundation mapping using NOAA AVHRR data, Water Resources Management, 20(6):949–959.

J.-H. Ryu, J.-S. Won and K.-D. Min, ''Waterline extraction from LandsatTM data in a tidal flat: A case study in Gomso Bay, Korea,'' Remote Sens. Environ, vol. 83, pp. 442–456, Dec. 2002, doi: 10.1016/S0034-4257(02)00059-7.

Ji et al., L. Ji, L. Zhang, B. Wylie. Analysis of dynamic thresholds for the normalized difference water index Photogrammetric Engineering and Remote Sensing, 75 (11) (2009), pp. 1307-1317, 10.14358/PERS.75.11.1307.

Lira, J. Segmentation and morphology of open water bodies from multispectral images. Int. J. Remote Sens 2006, 27, 4015–4038.

McFeeters, S. The use of the Normalized Difference Water Index (NDWI) in the delineation of open water features. *Int. J. Remote Sens* 1996, *17*, 1425–1432.

Rundquist, D., Lawson, M., Queen, L., and R. Cerveny, 1987, "The Relationship between Summer-Season Rainfall Events and Lake-Surface Area," Water Resources Bulletin, 23(3):493-508.

Rogers, A.S., and M.S. Kearney, 2004. Reducing signature variability in unmixing coastal marsh Thematic Mapper scenes using spectral indices, International Journal of Remote Sensing, 25(12):2317–2335.

Sethre, P.R.; Rundquist, B.C.; Todhunter, P.E. Remote detection of prairie pothole ponds in the Devil s Lake basin, North Dakota. GISci. Remote Sens. 2005, 42, 277–296, doi:10.2747/1548-1603.42.4.277.

Xu, H., Wang, X. & Zhang, X. Decreased vegetation growth in response to summer drought in Central Asia from 2000 to 2012. International journal of applied earth observation and geoinformation 52, 390–402 (2016).